Comparative Anatomy of Bat Jaw Musculature via Diffusible Iodine-Based Contrast-Enhanced Computed Tomography

SHARLENE E. SANTANA *
Department of Biology and Burke Museum of Natural History and Culture, University of Washington, Seattle, Washington, 98125

ABSTRACT

Noctilionoid bats exhibit an extraordinary array of cranial specializations that match diverse diets, including variation in jaw musculature physiological cross-sectional areas (PCSA), lever arms, and relative contribution to bite force. Although previous research in this group has linked variation in skull shape and muscle mechanics to biting performance, there are still important gaps about the anatomical underpinnings of noctilionoid dietary adaptations, including the degree of compartmentalization of the jaw musculature, and whether and how muscle attachment sites have evolved across noctilionoid species that specialize on derived diets. Here, we paired dissections with Diffusible Iodine-based Contrast-Enhanced Computed Tomography (diceCT) scanning in a comparative anatomical study of the jaw musculature of 12 noctilionoid species that span all diets found within the clade. We evaluated changes in jaw muscle attachments across species, identified differences in muscle compartments, examined scaling relationships, and compared the power of diceCT and dissections to generate morphological data. We found that diceCT enables more detailed investigation of muscle compartments and generates greater PCSA values, but these are strongly correlated with estimates from dissections. Jaw muscle origin and insertion sites are relatively conserved across noctilionoids when compared to other species-rich and ecologically-diverse mammalian groups. However, we found interspecific differences in the degree of separation of the *m. masseter*, and in the scaling relationships of different jaw muscles with body mass, both of which might be associated with diet and feeding behavior specialization. Our study highlights an unexplored diversity in the compartmentalization and fiber architecture of bat jaw muscles. Anat Rec, 301:267–278, 2018.

Key words: CT-scanning; feeding; Chiroptera; jaw adductors; PCSA; Phyllostomidae; Noctilionidae; Mormoopidae

The feeding apparatus of bats has undergone an extraordinary morphological diversification over the course of the lineage's radiation (Storch 1968; Freeman 1988; Dumont 2007). In particular, species within the Noctilionoidea have evolved the greatest diversity of cranial morphologies within mammals; the superfamily

Grant sponsor: National Science Foundation; Grant number: 1456375.

*Correspondence to: Sharlene E. Santana, Department of Biology, Kincaid Hall, Box 351800; Seattle, WA 98195-1800. Tel: +1-206-221-6888, E-mail: ssantana@uw.edu

Received 16 March 2017; Revised 31 July 2017; Accepted 24 August 2017.

DOI 10.1002/ar.23721

Published online in Wiley Online Library (wileyonlinelibrary.com).

includes species specialized in a wide variety of diets including insectivory, piscivory, carnivory, omnivory, frugivory, nectarivory, and sanguinivory. Noctilionoidea diverged from the rest of bats about 42.8–50.3 million years ago (Jones et al. 2005; Shi and Rabosky 2015), and is nested within the Yangochiroptera, a suborder that comprises most "microbat" families. It includes ≈207 species across three families with Neotropical distributions (Mormoopidae, Noctilionidae, and Phyllostomidae), and one family endemic to the islands of New Zealand (Mystacinidae) (Simmons 1998). Recent diversification analyses indicate that the only change in diversification rate across bats occurred within the noctilionoid family Phyllostomidae as a result of dietary evolution (Dumont et al. 2012; Shi and Rabosky 2015).

Although body mass explains a large amount of the variation in bite performance across noctilionoids and other bats (Herrel et al., 2008; Senawi et al., 2015; Santana and Miller, 2016), their jaw muscles vary significantly in terms of scaling relationships, physiological cross-sectional areas (PCSA), lever arms, and relative contribution to the forces required to open or close the jaw (Herrel et al. 2008; Santana et al. 2010; Santana and Curtis this issue). Noctilionoids that consume hard fruit and vertebrates have short and broad skulls with a high mechanical advantage, and their *m. temporalis* produces a greater moment about the temporomandibular joint (TMJ) relative to other jaw adductors (Herrel et al., 2008; Nogueira et al., 2009; Santana et al., 2012; Dumont et al., 2014; Santana and Cheung, 2016). In contrast, species that feed on softer diets have more elongated rostra, lower mechanical advantage, and a relatively higher contribution of other jaw adductors to the moment about the TMJ (Nogueira et al., 2009; Santana et al., 2010, 2012). The *m. temporalis* is the largest jaw adductor, and its mass scales with negative allometry across bats studied to date (Storch, 1968; Herrel et al., 2008); however, variation in *m. masseter* function (moment about the TMJ) explains the greatest amount of variation in bite force across noctilionoid species (Santana et al., 2010). This suggests that scaling, anatomical and physiological traits of individual jaw muscles also diversified in tandem with the dietary radiation of noctilionoids.

Although previous research has been able to connect variation in skull shape and muscle mechanics to biting performance, there are still important gaps in our understanding of the anatomical underpinnings of noctilionoid dietary adaptations. First, little is known about the degree of pennation in bat jaw adductors, as previous studies have separated these into their component parts to conduct bite force calculations (Herrel et al., 2008; Santana et al., 2010). Muscle pennation is common across vertebrate jaw adductors and enables greater packing of muscle fibers per unit of area, which allows the muscle to produce greater force for a given size (Gans, 1982; Otten, 1988). However, the angle of fiber pennation may also reduce force production in the muscle's direction of action (Gans, 1982; Otten, 1988; Perry et al., 2011; Gröning et al., 2013). Second, in the absence of comparative studies across noctilionoids, it is still unclear whether and how muscle origins and insertions have changed across species, or if they remain at conserved, homologous anatomical sites. These knowledge gaps are due, in part, to methodological difficulties posed by the small size of most bats.

In the past two decades, micro Computed-Tomography (μCT) scanning has become increasingly accessible. This has revolutionized the study of morphology by allowing researchers to reconstruct, measure, compare and model anatomical structures *in situ* with unprecedented detail, in three dimensions, and on relatively small organisms. More recently, there has been substantial progress in developing tools that allow imaging soft tissues via μCT scanning. These involve the use of contrast-enhancing staining agents (e.g., Lugol's iodine), which increase the radiodensities of some soft tissues so that they can be visualized in the same amount of detail as mineralized tissue (Metscher, 2009; Jeffery et al., 2011; Gignac and Kley, 2014). These methods, collectively known as Diffusible Iodine-based Contrast-Enhanced Computed Tomography (diceCT; Gignac et al. 2016), have already led to substantial progress in the study of muscle comparative anatomy, functional morphology, and biomechanics across a wide variety of taxa.

Here, we use diceCT scanning in a comparative anatomical study of the jaw musculature of 12 noctilionoid species. Our goals are to use 3D representations of the jaw musculature to (1) evaluate changes in origin and insertion sites across species that have different dietary specializations; (2) identify differences in *m. masseter* morphology, including compartmentalization (e.g., Storch 1968) and associated changes in fiber orientation across species; and (3) examine scaling relationships between muscle size, PCSA and body mass in the context of muscle compartmentalization and function. If dietary specialization has remodeled jaw muscle anatomy in noctilionoids, then species with highly derived diets (e.g., nectarivory, sanguinivory, frugivory) will differ from species with more conserved diets (e.g., insectivory) in muscle attachments and compartments. Furthermore, since bats are mass-constrained and fiber pennation alters the amount of force produced by a muscle, scaling relationships could differ among muscles that differ in their degree of pennation (e.g., to maximize bite force). Altogether, this exploration might help clarify previous findings regarding the importance of specific muscles in explaining bite force variation across species (Santana et al., 2010). In addition to anatomical comparisons, and due to the relative newness of diceCT, we also compare calculations of PCSAs derived from 3D data versus those from dissection data, and assess whether and how specimen characteristics may affect the application of the method. As the first diceCT study on the bat jaw musculature, we hope to contribute to the growing body of comparative 3D-imaging analyses of muscles in small vertebrates.

MATERIALS AND METHODS

Specimens, Imaging, and diceCT

To compare a wide diversity in cranial morphologies and dietary specializations, we examined fluid-preserved museum specimens belonging to 12 bat species across Noctilionoidea (Mormoopidae: 1 species; Noctilionidae: 1 species; Phyllostomidae: 10 species; Table 1, Fig. 5). We dissected the head of each specimen at the level of the atlas or axis vertebra and kept it in the original preserving fluid until the time of scanning. We used a Skyscan

TABLE 1. Specimen data for 12 bats included in the study

Species	Specimen Number	Locality	Collection Date	Original Preservation Method	Body mass (mg)	Days in Iodine	Scan Voxel Size (μm)
Noctilionidae							
Noctilio leporinus	PSM FHA1651	Dominican Republic	2-July-1968	70% ethanol	31.40	45	26.37
Mormoopidae							
Pteronotus parnellii	UWBM CR-022614-3	Costa Rica	26-Feb-2014	70% ethanol	15.25	21	19.7
Phyllostomidae							
Artibeus lituratus	AMNH 278258	Belize	4-May-2011	10% formalin	42.15	24	23.27
Artibeus phaeotis	AMNH 278321	Belize	4-May-2011	10% formalin	5.85	14	20.28
Brachyphylla nana	PSM FHA856	Dominican Republic	26-Sept-1967	70% ethanol	15.25	45	20.04
Carollia perspicillata	AMNH 278399	Belize	25-Apr-2012	10% formalin	10.50	12	20.04
Desmodus rotundus	AMNH 278331	Belize	5-May-2011	10% formalin	17.90	35	22.61
Glossophaga soricina	AMNH 278332	Belize	5-May-2011	10% formalin	4.05	10	14.56
Macrotus waterhousii	PSM FHA135	Dominican Republic	30-Jun-1962	70% ethanol	20.80	22	19.7
Micronycteris hirsuta	UWBM CR-030214-2	Costa Rica	2-Mar-2014	70% ethanol	14.60	18	23.31
Sturnira lilium	AMNH 278299	Belize	5-May-2011	10% formalin	10.55	14	17.31
Trachops cirrhosus	AMNH 278402	Belize	25-Apr-2012	10% formalin	25.00	35	20.28

Institution codes: AMNH = American Museum of Natural History, New York, NY; UWBM = University of Washington Burke Museum, Seattle, WA; PSM = Slater Museum of Natural History, Tacoma, WA.

1174 μCT-scanner (Bruker MicroCT, Belgium) for all the imaging procedures described in this study. We adjusted the scanning resolution to the minimum possible (14–30 μm voxel size, depending on specimen size), and ran all scans at 50 kV and 800 μA with a 0.25 mm aluminum filter. We scanned each specimen prior to iodine staining to facilitate segmentation of the cranium and mandible. We then submerged each bat head in a 1% w/v aqueous Lugol's iodine solution until all cranial muscles and their compartments were clearly visible in μCT cross sections (8–35 days; Table 1). We verified iodine uptake and muscle contrast levels by scanning each specimen every 3–5 days during the staining process, and refreshed the iodine solution as needed.

μCT Scan Reconstruction and PCSA Calculations

To examine muscle morphology and calculate PCSA from diceCT scans, we used the reconstruction software NRecon (Microphotonics Inc., Allentown, PA, USA) to convert the X-ray projection images produced by the μCT scanner into a volume consisting of a stack of X-ray attenuation cross sections ("slices"). We then imported the slices into Mimics v. 17.0 (Materialize, Ann Arbor, MI, USA) for digital segmentation of the skull and muscles. For μCT scans targeting the skull, we used Mimics' built-in threshold tool to isolate the range of grayscale values representing bone tissue. We then exported three-dimensional volume models of the crania and mandibles, respectively, as triangular surface meshes (.stl files). For the diceCT scans, we imported slices into Mimics, and manually outlined and segmented each individual jaw adductor and abductor muscle previously reported in Noctilionoids (*musculus masseter superficialis; m. masseter profundus; m. zygomaticomandibularis; m. temporalis: superficialis, medius, profundus and pars suprazygomatica; m. pterygoideus medius; m. pterygoideus lateralis*; and *m. digastricus*; Storch 1968; Herrel et al. 2008; Santana et al. 2010), along with visible parts of the skull. Each muscle was segmented as a separate unit if it was composed by a sheet of fibers following a similar orientation, bounded by fascia or bone surfaces (Hartstone-Rose et al., 2012). We created and exported triangular surface meshes (.stl files) for each individual muscle and uploaded these, along with the cranium and mandible .stl files, into Geomagic Studio (3D Systems, Rock Hill, SC). We used tools within this program to align the muscle and skulls meshes (based on dental and skull features), and to measure mesh volume. With these data, and fiber length data collected from dissections (below), we calculated Physiological Cross-sectional Areas for each muscle compartment (PCSA = muscle volume/fiber length). We used fiber length data from dissections because muscle fibers were not always clearly visible in our diceCT scans, resulting in less precise measurements, and specimens had been preserved at different gapes. To examine scaling relationships, we conducted Phylogenetic Generalized Least Squares (PGLS) regressions between $\log_{10}$-transformed muscle volumes and $\log_{10}$-transformed PCSA, respectively, and $\log_{10}$-transformed body mass (from specimen data). We used a Brownian correlation structure and a recent molecular phylogeny for these analyses (Dávalos et al., 2014).

Jaw Muscle Dissections

After completing diceCT scans, specimens were placed back in their preserving solution, which allowed most of the iodine to leach out over the course of a few days. We then dissected out the jaw musculature of each of these specimens to complement, compare and validate diceCT results. We took digital photos under a stereomicroscope (Leica M125, Leica Microsystems, Germany) at all stages of the dissection to qualitatively document muscle compartments, fascial planes, and origin and insertion areas. Upon dissection, we blotted the muscles dry and weighed them to the nearest 0.001g using an analytical balance (Mettler Toledo AE50, Mettler Toledo, Switzerland). To separate muscle fibers, we placed each muscle in a glass petri dish containing a 10% sulfuric acid solution, and heated it at 60°C inside a convection oven (VWR Symphony, VWR International, PA, USA) until muscle fibers could be easily separated (2–45 minutes, depending on muscle size and preservation condition; Perry et al. 2011). After chemical digestion, we transferred each muscle to a 50% glycerol (v/v) aqueous solution and used entomological needles to separate fiber bundles and individual muscle fibers under the stereomicroscope. We separated and took digital photos of 15 muscle bundles and fibers against a background grid, and used ImageJ (Rasband, W.S., ImageJ, U. S. National Institutes of Health, Maryland, USA) to measure their length to the nearest 0.01 mm. For each specimen and muscle compartment, we averaged muscle mass and fiber length measurements from the right and left side of the skull. We used these data to calculate Physiological Cross-sectional Areas (PCSA) for each jaw adductor (PCSA = muscle mass/(muscle density × fiber length); Lieber 2002; where density of the muscle tissue = 1.06 g/cm^3, Mendez and Keys 1960). We did not account for pennation angle in PCSA calculations angle because fiber pennation changes substantially and in three dimensions across jaw muscle sections and gapes, and this variation was not quantifiable from our diceCT scans. Additionally, muscles were separated into their component parts for fiber length quantification (Herrel et al. 2008). Similarly, we did not adjust PCSA estimates for sarcomere length, as transformations using an optimal length would not be adequate across specimens with different gapes and across muscle portions (Hartstone-Rose and Leischner, 2018; Hartstone-Rose et al., 2018). This, and the fact that only one individual represented each species, should be considered prior to using these PCSA values in future studies. We conducted paired t-tests comparing dissection and diceCT PCSA estimates, and carried out all statistical analyses in R (R Core Team, 2017).

Qualitative Analysis of Masseter Subdivisions

To visualize the degree of separation between the *m. masseter superficialis* and *profundus* in greater detail, we placed each right masseter in a 1% w/v aqueous Lugol's iodine solution for an additional 24–48 h after dissection and prior to chemical digestion (above). We scanned these isolated masseters at higher resolution using the Skyscan 1174 μCT scanner. As above, we reconstructed slices from shadow projection images in NRecon, and manually segmented these in Mimics v. 17.0 (Materialize, Ann Arbor, MI, USA).

RESULTS

Comparative Jaw Muscle Anatomy

Using diceCT scanning, we were able to visualize all jaw muscles previously described in bats (Fig. 1; Storch 1968). DiceCT allowed us to describe and/or revise muscle attachment areas and compartments more precisely than dissections, as the muscles remain *in situ* during digital segmentation. DiceCT was particularly useful for characterizing small muscles located more internally

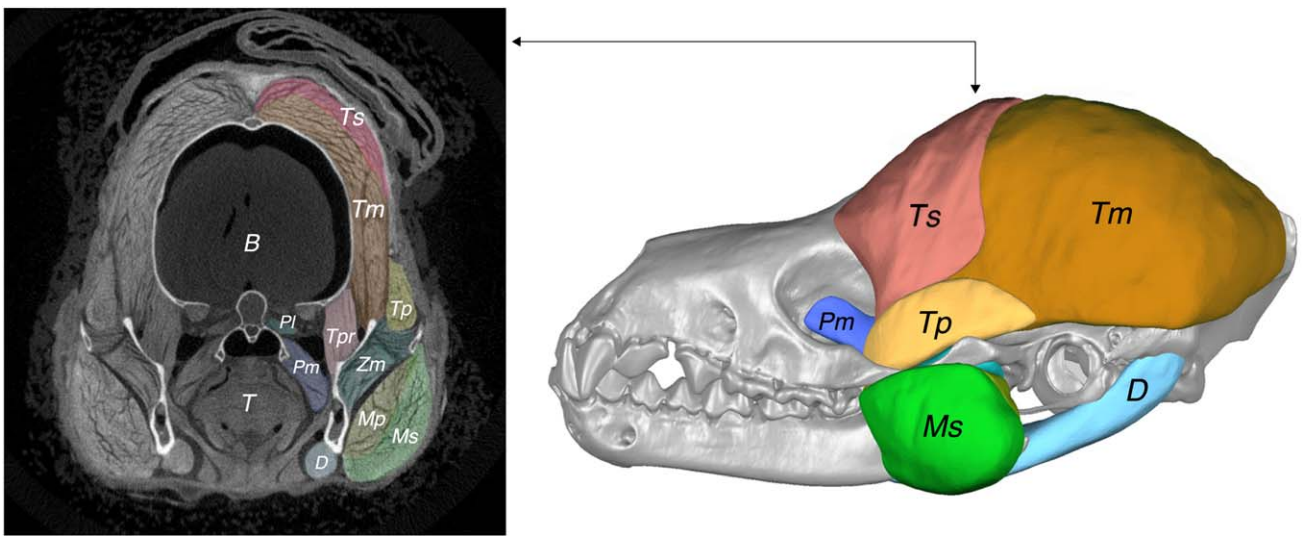

Fig. 1. Coronal section of a diceCT scan (left) and 3D reconstruction of the jaw musculature (right) in a representative noctilionoid, *Macrotus waterhousii*. *Ms: musculus masseter superficialis; Mp: m. masseter profundus; Zm: m. zygomaticomandibularis; Ts: m. temporalis superficialis, Tm: m. temporalis medius, Tpr: m. temporalis profundus; Tp: m. temporalis pars suprazygomatica; Pm: m. pterygoideus medius; Pl: m. pterygoideus lateralis*; *D: m. digastricus; T*: tongue; *B*: brain.

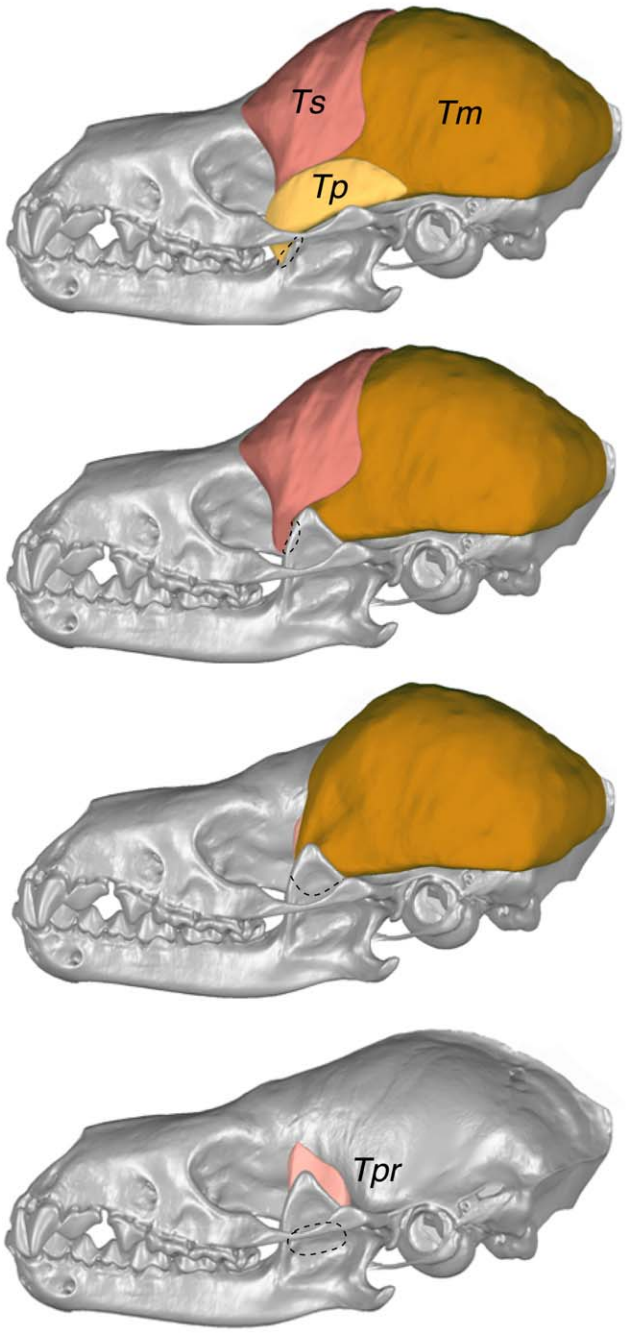

Fig. 2. 3D reconstruction of the *m. temporalis* in a representative noctilionoid, *Macrotus waterhousii. Ts: m. temporalis superficialis, Tm: m. temporalis medius, Tpr: m. temporalis profundus; Tp: m. temporalis pars suprazygomatica*. Muscle insertions areas in the mandible are indicated with a dashed line.

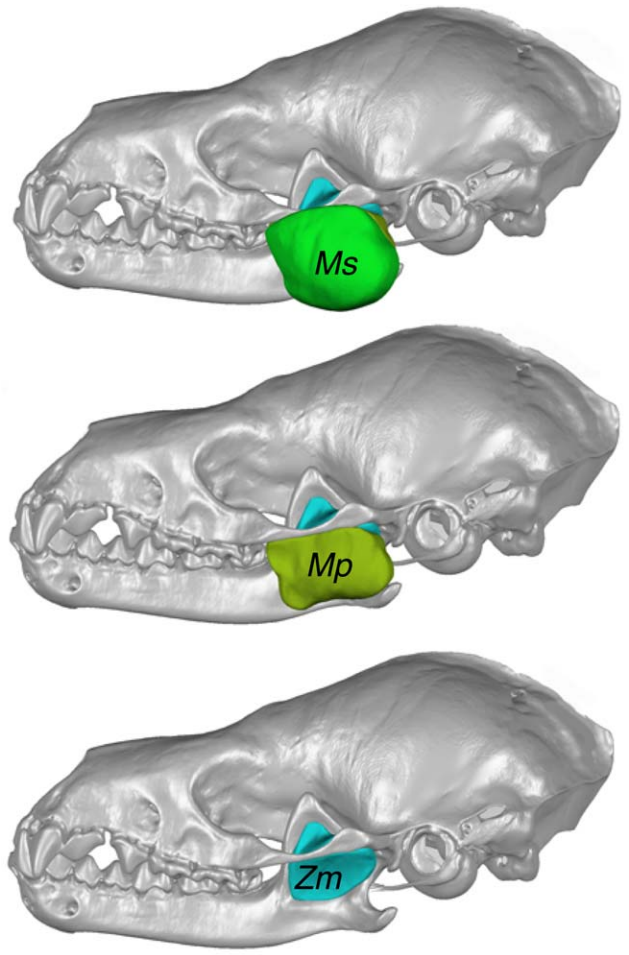

Fig. 3. 3D reconstructions of the *m. masseter superficialis* (*Ms*)*; m. masseter profundus* (*Mp*)*;* and *m. zygomaticomandibularis (Zm)* in a representative noctilionoid, *Macrotus waterhousii*.

(e.g., *m. temporalis profundus*; *m. pterygoideus medius* and *lateralis*), and incomplete subdivisions in some muscles (e.g., *m. masseter*, below). However, we were not able to reliably measure fiber lengths from our μCT scans because they did not have sufficient resolution, and specimens had been preserved at different gapes. Despite these challenges, we were able to discern general patterns of fiber orientation in the larger muscles of most specimens. Below we detail our diceCT findings on jaw muscle anatomy across the bat species studied. These are illustrated in a representative noctilionoid, *Macrotus waterhousii*, in Figures 1–4.

The *m. temporalis*, the largest jaw adductor across all species (Tables 2 and 3), has four major compartments (*superficialis, medius, profundus, pars suprazygomatica*) that were clearly visible using diceCT. In almost all bats examined, a sheet of muscle fibers forming the *m. temporalis superficialis* originates from the frontal region, expands caudally following the skull's midline to about a third of the braincase's length (covering the anterior portion of the *m. temporalis medius*), and inserts on the anterior margin of the coronoid process of the mandible (Figure 2). The *m. temporalis medius* originates from the lateral surface of the braincase, extending to the midline and the sagittal crest, and inserts on the medial surface of the coronoid process, immediately dorsal to the insertion of the *m. temporalis profundus*. The latter originates from the ventral portion of the frontal and inserts above the mandibular foramen's dorsal ridge. These *temporalis* attachment patterns are common across all the species studied with two exceptions: (1) in

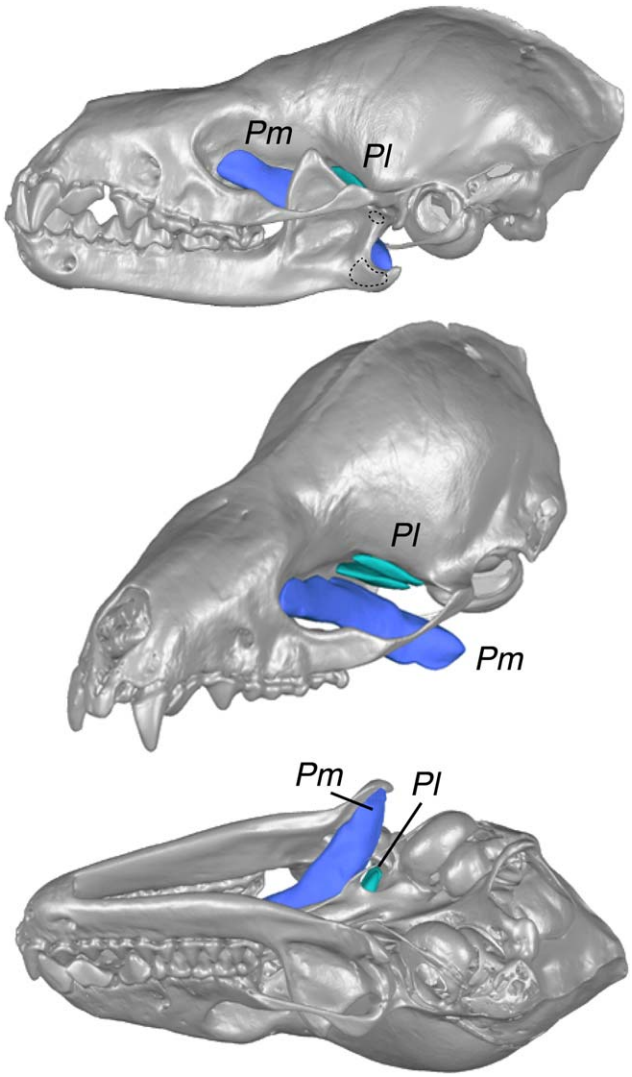

Fig. 4. 3D reconstruction of the *m. pterygoideus medius* (*Pm*) and *m. pterygoideus lateralis* (*Pl*) in a representative noctilionoid, *Macrotus waterhousii*, showing origins in the cranium and insertions in the mandible.

G. soricina the *temporalis* complex is reduced in size such that neither the *m. temporalis superficialis* nor the *m. temporalis medius* reach the midline of the cranium, and (2) in *N. leporinus* the *m. temporalis superficialis*' fascia attaches throughout the length of the braincase, including the sagittal crest (Fig. 5). The *m. temporalis pars suprazygomatica* originates anteriorly from the medial, posterior margin of the zygomatic arch and posteriorly from the superior surface of the squamous-temporal bone above the TMJ, and inserts on the on the antero-dorsal margin of the coronoid process. The *pars suprazygomatica* is absent in *G. soricina* and *N. leporinus*, but can be relatively large in some species such that it protrudes well behind and above the zygomatic arch (e.g., *M. waterhousii, M. hirsuta;* Fig. 5).

μCT scans of the *m. masseter* at higher resolution allowed us to assess the degree of separation between its superficial and deep compartments across species (Fig. 6). With the exception of *D. rotundus*, where we could not discern clear subdivision (Fig. 6A), all species appear to have at least some separation between the two compartments; we observed a fascial plane that extends from the insertion of the muscle to about one quarter to half of its length (Fig. 6B, 6C). In a few species (*N. leporinus, M. waterhousii, M. hirsuta*), we also noted an anterior fascial plane dividing the compartments (Fig. 6C), but we could not discern if it was continuous with the posterior plane. Across species, the more superficial fibers of the masseter originate from the ventral, and slightly lateral portion of the zygomatic arch, with fibers running diagonally in an antero-posterior direction towards the insertion in the angular process. Deeper masseter fibers run in a similar fashion but originate more posteriorly and medially on the zygomatic arch, and insert at a higher point in the ramus (bound dorsally by the masseteric fossa). Notably, we find the same masseter arrangement described above in *C. perspicillata*, even though this bat lacks an ossified zygomatic arch (Figs. 3 and 6B).

Across all species, the *m. zygomaticomandibularis* originates from the medial surface and posterior third of the zygomatic arch, and inserts in the masseteric fossa (Fig. 3). DiceCT scans revealed that the *m. pterygoideus lateralis* is composed of two, minuscule compartments, which originate from a groove on the lateral surface of the palatine-pterygoid bones, and insert on the ventral surface of the neck of the mandibular condyle (Fig. 4). The relatively larger *m. pterygoideus medius* originates anterior to the *m. pterygoideus lateralis* from a fossa on the lateral surface of the palatine, follows the curvature of the pterygoid posteriorly, and inserts on the medial surface of the angular process (Fig. 4). A tendinous sling connecting the *m. pterygoideus medius* and the *m. masseter* was visible on dissections but not on diceCT scans.

Dissections indicate that the jaw abductor, *m. digastricus*, is formed by two bellies. However, these are tightly connected and we were not able to segment them as separate units in diceCT scans. As a whole, the digastric originates from deep grooves in the mastoid notch, and inserts on the ventral surface of the posterior third of the mandibular ramus (also see Curtis and Santana, 2018, for more details on digastric variation across noctilionoids).

Muscle Scaling

Scaling relationships using diceCT-derived data are shown in Tables 4 and 5. The volumes and PCSAs of all jaw muscles exhibit positive slopes with respect to body mass. However, the PCSA of the *m. temporalis medius* is the only variable that scales with significant positive allometry with respect to body mass (Table 5); the slopes and confidence intervals for the volumes and PCSAs of all other jaw muscles included values that were lower than the isometric prediction (1, Table 4; 0.67, Table 5), suggesting negative allometry.

Methodological Findings

Pair-wise comparisons revealed statistically significant differences in PCSA calculated from dissection versus diceCT data (paired t-test: $t = 6.035$, $df = 11$, $P = 8.483 \times 10^{-05}$). DiceCT-derived data produced

TABLE 2. Specimen jaw muscle Physiological Cross-Sectional Areas (PCSA, in mm^2) calculated from dissection data

Species	Temporalis				Masseter	Zygom.	Medial Pterygoid	Lateral Pterygoid	Digastric
	Sup.	Med.	Deep	Pars supra					
Noctilionidae									
Noctilio leporinus	51.07	35.02	2.63	–	6.37	6.14	5.71	2.97	2.80
Mormoopidae									
Pteronotus parnellii	7.46	42.69	2.01	0.7	7.98	2.58	4.34	1.59	1.68
Phyllostomidae									
Artibeus lituratus	13.35	46.05	4.18	1.54	7.27	5.07	5.1	1.82	3.98
Artibeus phaeotis	3.55	9.09	1.18	0.34	1.89	1.86	2.71	1.65	0.87
Brachyphylla nana	5.43	19.27	2.39	0.98	9.21	2.03	5.2	1.41	1.69
Carollia perspicillata	3.60	14.23	0.76	0.23	6.25	1.01	2.98	0.84	1.57
Desmodus rotundus	2.32	22.98	1.71	0.45	4.17	2.34	4.26	1.53	2.71
Glossophaga soricina	2.13	3.78	1.00	–	1.5	0.63	1.78	0.71	0.78
Macrotus waterhousii	7.91	40.37	1.97	1.61	14.3	2.25	4.78	1.01	2.00
Micronycteris hirsuta	5.68	42.55	2.03	1.05	9.95	1.8	1.77	1.18	1.55
Sturnira lilium	1.89	11.02	1.20	0.2	4.91	0.98	2.74	1.68	2.13
Trachops cirrhosus	6.20	30.32	2.56	0.77	6.42	2.58	4.32	2.14	2.39

TABLE 3. Specimen jaw muscle Physiological Cross-Sectional Areas (PCSA, in mm^2) calculated from diceCT

Species	Temporalis				Masseter	Zygom.	Medial Pterygoid	Lateral Pterygoid	Digastric
	Sup.	Med.	Deep	Pars supra					
Noctilionidae									
Noctilio leporinus	67.99	35.47	3.53	–	5.50	7.30	7.10	3.50	2.14
Mormoopidae									
Pteronotus parnellii	9.04	42.04	2.31	0.30	7.20	2.80	6.00	2.10	1.40
Phyllostomidae									
Artibeus lituratus	14.01	45.77	6.06	1.80	9.20	6.40	6.90	2.90	4.61
Artibeus phaetois	4.98	12.07	2.23	0.19	3.10	2.46	3.04	1.59	1.10
Brachyphylla nana	7.28	23.11	4.86	0.90	8.80	3.40	7.10	2.50	1.69
Carollia perspicillata	4.97	17.50	0.95	0.30	7.30	1.20	3.50	0.80	1.54
Desmodus rotundus	4.68	29.03	3.67	0.50	5.60	5.40	8.20	2.40	3.51
Glossophaga soricina	2.21	5.98	0.45	–	1.40	0.80	1.80	0.80	0.81
Macrotus waterhousii	10.50	43.54	2.81	2.00	15.90	3.50	5.50	1.10	1.96
Micronycteris hirsuta	8.95	51.16	2.53	1.30	10.20	4.00	2.50	1.30	1.62
Sturnira lilium	4.19	12.67	1.68	0.20	6.20	1.60	3.60	2.10	2.66
Trachops cirrhosus	8.43	36.13	3.60	1.00	7.90	4.10	7.00	3.30	2.30

consistently greater PCSA estimates than dissection-derived data (Tables 2 and 3). Nevertheless, dissection and diceCT PCSA estimates were strongly and significantly correlated, and their regression had a slope not significantly different from one (Fig. 7; $b = 1.102 \pm 0.058$; $t = 18.695$, $R^2 = 0.969$, $df = 10$, $P = 4.15 \times 10^{-09}$).

Specimen age, total muscle mass, and preservation method (from Table 1) did not have a statistically significant effect on the staining times across the specimens examined (specimen age: $b = 0.001 \pm 0.0009$, $t = 1.151$, $P = 0.283$; total muscle mass: $b = 21.946 \pm 13.769$, $t = 1.594$, $P = 0.150$; specimen age $\times$ total muscle mass: $b = 6.267 \times 10^{-04} \pm 14.526 \times 10^{-04}$, $t = -0.431$, $P = 0.678$; preservation method: $F = 1.880$, $P = 0.200$). However, some of the older and larger, ethanol-preserved specimens took longer to stain (Fig. 8). We did not observe any differences in the quality of final diceCT scans that seemed related to specimen age or preservation method, but formalin-preserved specimens appeared to maintain better muscle integrity after iodine staining.

DISCUSSION

Our diceCT findings are consistent with our observations from dissections and previous gross anatomy descriptions of the bat jaw musculature (e.g., Storch 1968, who described the cranial musculature of five species included in our sample and other bats; Herrel et al. 2008; Senawi et al. 2015). However, diceCT revealed finer details of muscle arrangements, attachments, and subdivisions, which highlights the utility of this method for describing and quantifying the anatomy of small muscles. As a non-destructive method, diceCT allowed us to visualize and compare muscle characteristics *in situ*, and side-by-side among species.

Noctilionoid bats exhibit the greatest diet diversity across mammals, yet our results indicate that—with few exceptions—jaw muscle origins and insertion sites are relatively conserved across the species examined. Comparisons with previous anatomical descriptions also highlight similarities between noctilionoids and other

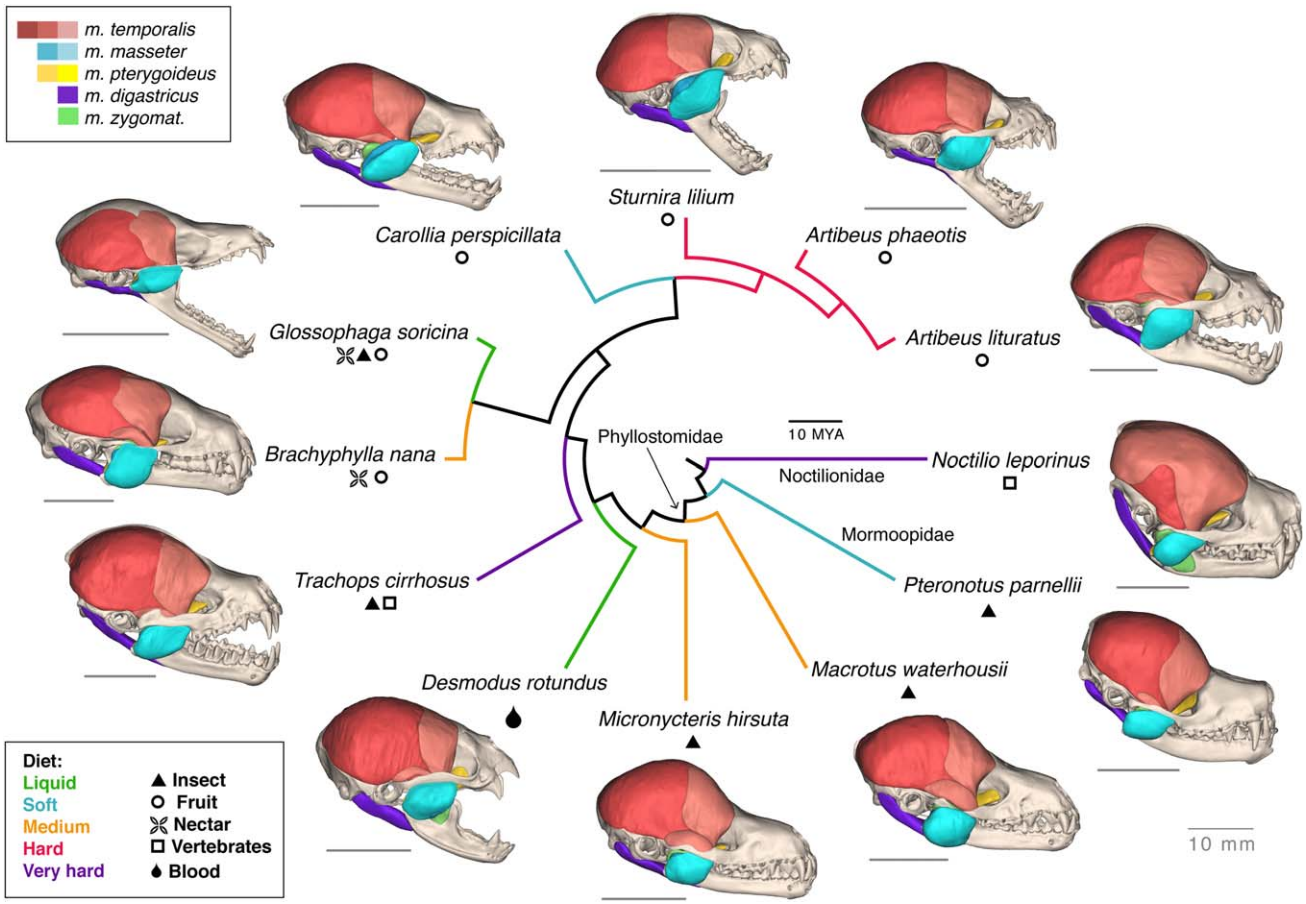

Fig. 5. 3D reconstructions of the jaw musculature across noctilionoid species studied, in the context of their evolutionary relationships.

bats in these muscle attachment sites. For example, the distantly related frugivorous species, *Pteropus giganteus* (Pteropodidae; Suborder Yinpterochiroptera), exhibits muscle compartments and attachment sites almost identical to those found in most noctilionoids (De Gueldre and De Vree, 1988). However, certain jaw adductors also seem to differ markedly across bat species; the *m. temporalis profundus* appears to be absent in *Myotis myotis* (Vespertilionidae) and *Taphozous nudiventris* (Emballonuridae) (Storch 1968), although it is unclear if the small sizes of these bats create challenges in identifying these compartments. Furthermore, the size of the area from which the *m. masseter* and *zygomaticomandibularis* originate also seems to vary across bats (e.g., from about one-third to half of the length of the zygomatic arch; Storch 1968). Altogether, these trends seem to broadly reflect phylogenetic patterns observed in other mammalian groups, in which muscle attachment sites remain generally consistent at the family level but are more disparate at higher taxonomic levels (Druzinsky et al. 2011). From an ecological perspective, jaw adductor attachments in noctilionoids seem to be more conserved than in other species-rich and ecologically-diverse mammalian lineages; jaw adductor origins and insertions are dramatically different among major rodent clades that are specialized for different masticatory demands (e.g., hystricomorph and sciuromorph masseter arrangements for grinding and gnawing, respectively, Cox et al. 2012).

With the exception of nectarivorous species, in which the jaw musculature is reduced in size, the dietary radiation of noctilionoids seems to have evolved within a relatively consistent template of muscle attachment sites. Within this template, and as noctilionoids radiated under various selective regimes on bite performance (Dumont et al., 2014), the jaw musculature likely helped reshape the bones on which they attach, and vice versa (Ravosa et al., 2008; Anderson et al., 2014). As differences in jaw adductor PCSA, and cranium and mandible shape are highly correlated with bite performance in noctilionoids (Santana et al., 2010; Dumont et al., 2012), it is possible that the feeding system has evolved in a highly integrated fashion in this clade. Future studies should investigate this possibility through comparative anatomical analyses within macroevolutionary and developmental frameworks.

Our study highlights the potential for undescribed diversity in the compartmentalization and fiber architecture of noctilionoid jaw muscles. Although most of our μCT scans lacked the resolution needed to discern individual muscles fibers precisely, diceCT scans complemented with dissections clearly indicated that several

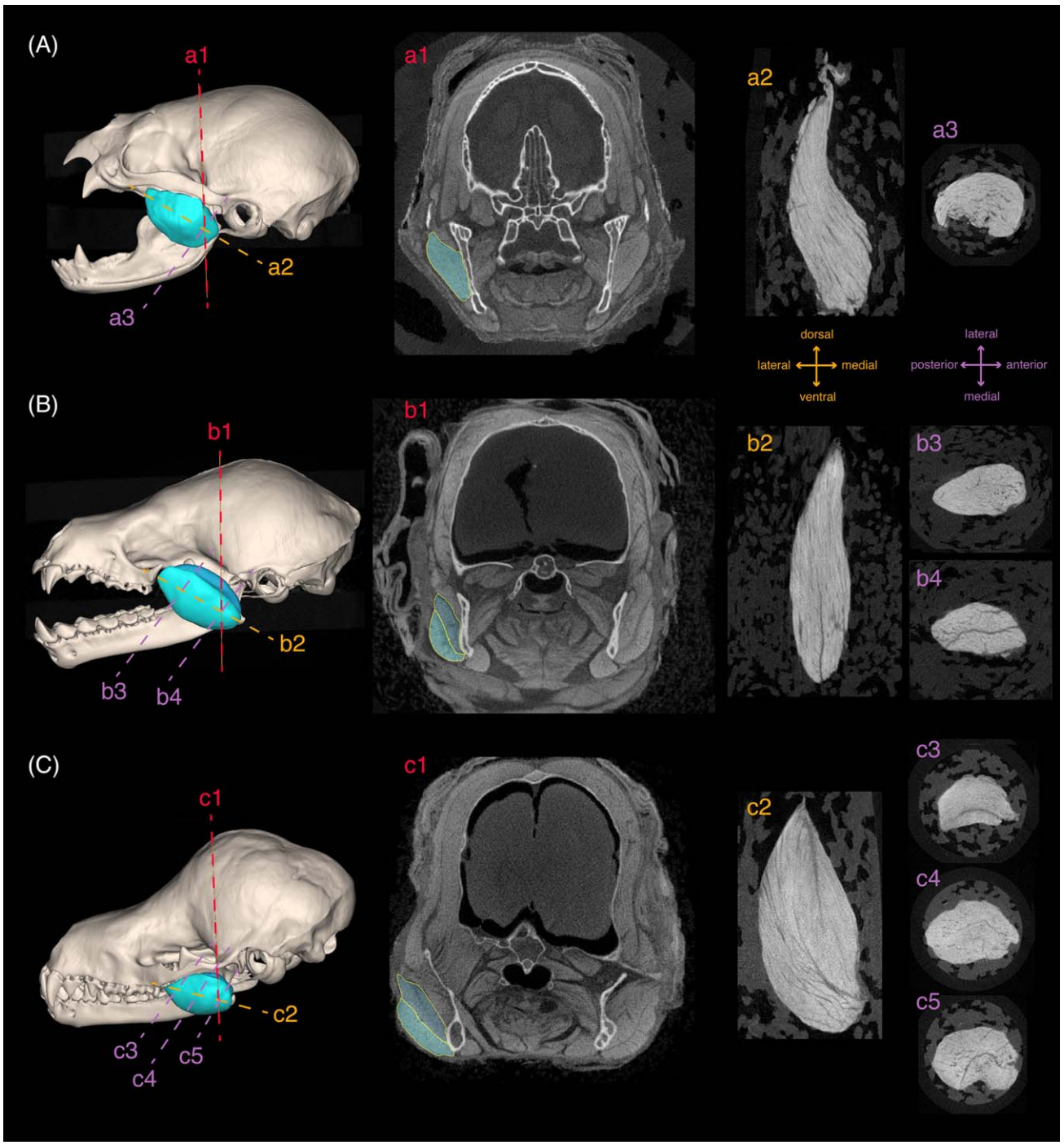

Fig. 6. DiceCT scans of three representative noctilionoids illustrating variation in the degree of compartimentalization of the *m. masseter*; (**A**) *Desmodus rotundus*: no separation between the *m. masseter superficialis* and the *m. masseter profundus*; (**B**) *Carollia perspicillata*: posterior separation; (**C**) *Micronycteris hirsuta*: anterior and posterior separation. From left to right: 3D reconstructions of the *m. masseter* and the skull showing section planes; coronal sections at the posterior end of the *m. masseter*; oblique sections at the greatest length of the *m. masseter*, from diceCT scans of dissected masseters; and axial sections from diceCT scans of dissected masseters.

jaw muscles are subdivided by fascial planes into distinct compartments. The *m. temporalis* is one of such muscles; it is composed by four distinct subdivisions (*superficialis, medius, profundus* and *pars suprazygomatica*). Complete separation among these compartments, as well as differences in their relative size (Fig. 5, Tables 2 and 3), highlights the potential for functional subdivision within this muscle. For example, these could provide finer directionality during mandible elevation depending on which parts of the *temporalis* are active.

TABLE 4. Scaling slopes for the volume of each jaw muscle across noctilionoid bats

Volume	b	(Lower limit–Upper limit)	t	P
m. temporalis				
superficialis	0.715	(0.714–0.716)	2.282	0.0456
medius	0.856	(0.775–0.937)	10.116	<0.0001
profundus	0.901	(0.736–1.066)	5.462	0.0003
pars suprazygomatica	1.264	(0.991–1.537)	4.625	0.0017
m. masseter	0.737	(0.632–0.843)	6.998	<0.0001
m. zygomaticomandibularis	0.719	(0.600–0.839)	6.022	0.0001
m. pterygoideus				
medius	0.709	(0.596–0.823)	6.253	0.0001
lateralis	0.771	(0.636–0.906)	5.717	0.0002
m. digastricus	0.954	(0.909–0.999)	21.212	<0.0001

Results are for a phylogenetic generalized least-squares regression where Log_{10} muscle volume = $Log_{10}a + b\ Log_{10}$(body mass). The expected slope under isometry is 1. P-values correspond to the significance of the regression. Volumes for the two compartments of the *m. pterygoideus lateralis* and the *m. digastricus* were combined, as were the two compartments of the masseter in the species where they were present.

TABLE 5. Scaling slopes for the Physiological Cross-Sectional Area (PCSA) of each jaw muscle across noctilonoid bats

PCSA	b	(Lower limit–Upper limit)	t	P
m. temporalis				
superficialis	0.705	(0.545–0.864)	4.418	0.0013
medius	0.776	(0.677–0.886)	7.096	<0.0001
profundus	0.790	(0.613–0.966)	4.471	0.0012
pars suprazygomatica	0.586	(0.431–0.741)	3.780	0.0054
m. masseter	0.659	(0.508–0.809)	4.365	0.0014
m. zygomaticomandibularis	0.700	(0.566–0.835)	5.210	0.0004
m. pterygoideus				
medius	0.546	(0.437–0.654)	5.031	0.0005
lateralis	0.452	(0.314–0.590)	3.280	0.0083
m. digastricus	0.656	(0.563–0.749)	7.049	<0.0001

Results are for a phylogenetic generalized least-squares regression where Log_{10} PCSA = $Log_{10}a + b\ Log_{10}$(body mass). The expected slope under isometry is 0.67. P-values correspond to the significance of the regression. PCSAs for the two compartments of the *m. pterygoideus lateralis* and the *m. digastricus* were combined, as were the two compartments of the masseter in the species where they were present.

Similarly, subdivisions within the *m. pterygoideus* group may indicate specializations for different degrees of mandible adduction, abduction, protrusion and lateral excursion. Although there are no published electromyography data on noctilionoid jaw muscles, studies on Indian flying foxes (*Pteropus giganteus*) indicate that asynchronous and asymmetric contraction of jaw muscles and their parts are responsible for precise mandible movements during mastication (De Gueldre and De Vree, 1988). Asymmetric activity in the *m. masseter* and *m. pterygoideus medius* causes subtle protrusion of the mandible during early opening, whereas lateral excursions at the end of opening and at the start of closing are caused by asymmetric and asynchronous activity in the *m. pterygoideus* and *m. digastricus*, and by asynchronous activation of the *m. temporalis profundus* and the *m. zygomaticomandibularis*.

Through a more detailed diceCT analysis, we were able to identify compartments of the *m. masseter* previously named in other mammals (e.g., felids, Hartstone-Rose et al. 2012; primates, Perry et al. 2011; rodents Cox et al. 2012, Baverstock et al. 2013): *superficialis* and *profundus*, which varied their degree of separation (Fig. 6), and a distinct and separate *m. zygomaticomandibularis*. The observed variability in the subdivision of the *m. masseter* is consistent with comparative analyses in other mammals (reviewed in Druzinsky et al. 2011), as is the tendinous connection between the insertions of the *m. masseter superficialis* and the *m. pterygoideus medius*. Differences in masseter pennation may either increase or decrease muscle force depending on the angle of fiber orientation with respect to the axis of muscle action (Gans, 1982; Otten, 1988; Perry et al., 2011; Gröning et al., 2013), and may help explain why this muscle has different scaling relationships than other major jaw adductors (below). A more detailed anatomical analysis measuring fiber lengths and pennation angle within each compartment, and across multiple individuals per species, is needed to identify the potential impact of masseter fiber architecture on bite force production in bats. This is possible via diceCT using equipment with a higher power source and resolution (Metscher 2009; Santana et al. in prep.).

Previous studies of noctilionoid feeding biomechanics have demonstrated differences in the relative importance of specific jaw adductors and their lever mechanics on bite force production, with hard-diet species having larger *temporalis* complexes and a greater moment about the TMJ produced by these muscles (see Herrel

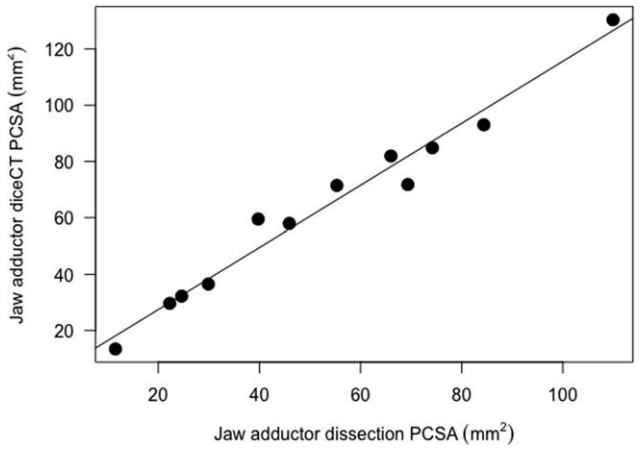

Fig. 7. Regression of jaw adductor Physiological Cross-Sectional Area (PCSA) calculated using data from dissections (muscle mass) versus PCSA calculated from diceCT data (muscle volume). Regression line: $b = 1.102 \pm 0.058$; $t = 18.695$, $R^2 = 0.969$, $df = 10$, $P = 4.15 \times 10^{-09}$.

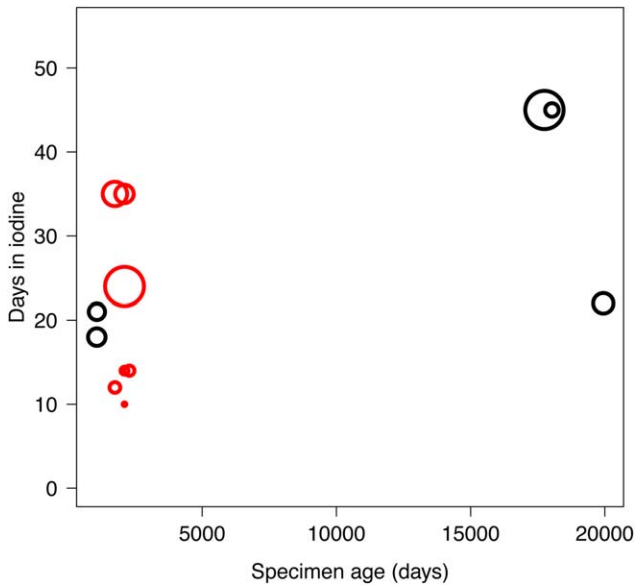

Fig. 8. Specimen age versus days in iodine until muscle contrast was achieved in diceCT scans. Data points are scaled to reflect total jaw muscle mass of each specimen. Red: formalin-preserved specimens, black: ethanol-preserved specimens.

et al., 2008; Santana et al., 2010 for detailed asssessments of skull and muscle mechanics in noctilionoids and other bats). As the largest species in our dataset feed on mechanically challenging food items (*Noctilio leporinus*: fish; *Trachops cirrhosus*: vertebrates; *Artibeus lituratus*: hard fruit), it not surprising that the PCSA of the largest section of the *temporalis* scales with positive allometry—larger, hard-diet species possess relatively larger *m. temporalis medius* for their size, which would confer them with disproportionally higher bite forces at wide gapes to acquire and process large and/or tough food items (Santana and Cheung, 2016). In sharp contrast, the volumes and PCSAs of the rest of the jaw muscles scale with isometry or negative allometry. That is, larger species have relatively similar or smaller PCSAs of these muscles for their size (conversely, smaller species have relatively larger volumes and PCSAs of these muscles). A nectarivore (*Glossophaga soricina*) and a frugivore that consumes soft-fruit (*Carollia perspicillata*) are among the smallest species in our dataset. Both of these species primarily use molar bilateral bites when consuming fruit (Dumont, 1999; Santana and Dumont, 2009). The relatively larger *masseter* in these species may provide greater biting strength at narrower gapes and aid in mandible protrusion, whereas a larger *zygomaticomandibularis* and *pterygoideus* may be advantageous for lateral excursion of the mandible. The latter may be especially important in *C. perspicillata*, as this species uses side-to-side biting motions to feed on the cylindrically-shaped *Piper* infructescences that make up the bulk of its diet (Heithaus, 1982).

From a methodological perspective, we did not find an effect of specimen size or preservation fluid type on the staining times required to produce clear contrast among jaw muscles. However, our specimens were relatively small, with total muscle masses only ranging between 0.1-1 g. Larger specimens still remain a challenge for diceCT (Gignac et al., 2016), as does the time required to perform digital segmentation and measure muscle fibers and their orientations. Although our sample was limited, we found a strong correlation between PCSA estimates from diceCT and dissections, with diceCT providing consistently greater estimates. These estimates were also consistent with previously reported values for some of the species under study (Herrel et al. 2008; Santana et al. 2010). This is an encouraging finding, since ethanol preservation may produce tissue shrinkage (Vickerton et al. 2013) and therefore reduce PCSA estimates, and iodine staining could lead to a slight increase in muscle mass due to iodine intake. Altogether, our results highlight the potential of diceCT as a promising tool for resolving fiber architecture (e.g., by μCT scanning specimens at a higher resolution), defining muscle attachments more accurately, and providing data to inform functional morphology studies that model bite performance. It remains critical, however, to validate diceCT results with traditional methods such as dissections, to corroborate and expand the results generated with this emerging tool.

ACKNOWLEDGMENTS

I would like to thank Abby Vander Linden for μCT scanning and data collection; Brie Ilarde for help with data collection on muscle fiber length; Dr. Nancy Simmons at the American Museum of Natural History and Gary Shugart at the Slater Museum of Natural History for providing access to specimens; Paul Gignac for diceCT tips; Raj Manoharan and Ian Spradlin at Microphotonics for assistance with μCT-scanning issues; and two anonymous reviewers for constructive criticism.

LITERATURE CITED

Anderson PSL, Renaud S, Rayfield EJ. 2014. Adaptive plasticity in the mouse mandible. BMC Evol Biol 14:85.

Baverstock H, Jeffery NS, Cobb SN. 2013. The morphology of the mouse masticatory musculature. J Anat 223:46–60.

Cox PG, Rayfield EJ, Fagan MJ, Herrel A, Pataky TC, Jeffery N. 2012. Functional evolution of the feeding system in rodents. PLoS One 7:e36299.

Curtis AA, Santana SE. 2018. Jaw-dropping: functional variation in the digastric muscle in bats. Anat Rec 301:279–290.

Dávalos LM, Velazco PM, Warsi OM, Smits PD, Simmons NB. 2014. Integrating incomplete fossils by isolating conflicting signal in saturated and non-independent morphological characters. Syst Biol 63:582–600.

De Gueldre G, De Vree F. 1988. Quantitative electromyography of the masticatory muscles of *Pteropus giganteus* (Megachiroptera). J Morphol 196:73–106.

Druzinsky RE, Doherty AH, De Vree FL. 2011. Mammalian masticatory muscles: homology, nomenclature, and diversification. Integr Comp Biol 51:224–234.

Dumont ER, Dávalos LM, Goldberg A, Santana SE, Rex K, Voigt CC. 2012. Morphological innovation, diversification and invasion of a new adaptive zone. Proc R Soc B Biol Sci 279:1797–1805.

Dumont ER, Samadevam K, Grosse I, Warsi OM, Baird B, Dávalos LM. 2014. Selection for mechanical advantage underlies multiple cranial optima in new world leaf-nosed bats. Evolution 68:1436–1449.

Dumont ER. 1999. The effect of food hardness on feeding behaviour in frugivorous bats (Phyllostomidae): an experimental study. J Zool 248:219–229.

Dumont ER. 2007. Feeding mechanisms in bats: variation within the constraints of flight. Integr Comp Biol 47:1–10.

Freeman PW. 1988. Frugivorous and animalivorous bats (Microchiroptera) - dental and cranial adaptations. Biol J Linn Soc 33:249–272.

Gans C. 1982. Fiber architecture and muscle function. Exerc Sport Sci Rev 10:160–207.

Gignac PM, Kley NJ, Clarke JA. 2016. Diffusible iodine-based contrast-enhanced computed tomography (diceCT): an emerging tool for rapid, high-resolution, 3-D imaging of metazoan soft tissues. J Anat 1–119.

Gignac PM, Kley NJ. 2014. Iodine-enhanced micro-CT imaging: methodological refinements for the study of the soft-tissue anatomy of post-embryonic vertebrates. J Exp Zool B Mol Dev Evol 322:166–176.

Gröning F, Jones MEH, Curtis N, Herrel A, O'Higgins P, Evans SE, Fagan MJ. 2013. The importance of accurate muscle modelling for biomechanical analyses: a case study with a lizard skull. J R Soc Interface 10:20130216.

Hartstone-Rose A, Deutsch A, Leischner C, Pastor J. 2018. Dietary and phylogenetic correlates of primate masticatory muscle fiber architecture. Anat Rec 301:311–324.

Hartstone-Rose A, Leischner CL. 2018. Feeding adaptations of the primate skull and masticatory muscles In: Lambert JE, Rothman J, editors. Primate diet and nutrition: needing, finding, and using food.

Hartstone-Rose A, Perry JMG, Morrow CJ. 2012. Bite force estimation and the fiber architecture of felid masticatory muscles. Anat Rec 295:1336–1351.

Heithaus ER. 1982. Coevolution between bats and plants. In: Kunz TH, editor. Ecology of bats. NY: Springer. p 327–367.

Herrel A, De Smet A, Aguirre LF, Aerts P. 2008. Morphological and mechanical determinants of bite force in bats: do muscles matter? J Exp Biol 211:86–91.

Jeffery NS, Stephenson RS, Gallagher JA, Jarvis JC, Cox PG. 2011. Micro-computed tomography with iodine staining resolves the arrangement of muscle fibres. J Biomech 44:189–192.

Jones KE, Bininda-Emonds ORP, Gittleman JL. 2005. Bats, clocks, and rocks: diversification in patterns in Chiroptera. Evolution 59: 2243–2255.

Lieber RL. 2002. Skeletal muscle structure, function and plasticity: the physiological basis of rehabilitation. Baltimore: Lippincott Williams & Wilkins.

Mendez J, Keys A. 1960. Density and composition of mammalian muscle. Metabolism 9:184–188.

Metscher BD. 2009. MicroCT for comparative morphology: simple staining methods allow high-contrast 3D imaging of diverse non-mineralized animal tissues. BMC Physiol 9:11.

Nogueira MR, Peracchi AL, Monteiro LR. 2009. Morphological correlates of bite force and diet in the skull and mandible of phyllostomid bats. Funct Ecol 23:715–723.

Otten E. 1988. Concepts and models of functional architecture in skeletal muscle. Exerc Sport Sci Rev 16:98–138.

Perry JMG, Hartstone-Rose A, Wall CE. 2011. The jaw adductors of strepsirrhines in relation to body size, diet, and ingested food size. Anat Rec 294:712–728.

Ravosa MJ, Kunwar R, López EK, Klopp EB, Pinchoff J, Stock SR, Stack MS, Hamrick MW. 2008. Adaptive plasticity in the mammalian masticatory complex: you are what, and how, you eat. In Vinyard CJ, Ravosa MJ, and Wall CE, editors. Primate cranofacial function and biology. NY: Springer. p. 293–328.

R Core Team. 2017. R: A language and environment for statistical computing. R Foundation for Statistical Computing, Vienna, Austria. URL http://www.R-project.org/.

Santana SE, Cheung E. 2016. Go big or go fish: morphological specializations in carnivorous bats. Proc R Soc B Biol Sci 283: 20160615.

Santana SE, Dumont ER, Davis JL. 2010. Mechanics of bite force production and its relationship to diet in bats. Funct Ecol 24:776–784.

Santana SE, Dumont ER. 2009. Connecting behaviour and performance: the evolution of biting behaviour and bite performance in bats. J Evol Biol 22:2131–2145.

Santana SE, Grosse IR, Dumont ER. 2012. Dietary hardness, loading behavior, and the evolution of skull form in bats. Evolution 66:2587–2598.

Santana SE, Miller K. 2016. Extreme postnatal scaling in bat feeding performance: a view of ecomorphology from ontogenetic and macroevolutionary perspectives. Integr Comp Biol 56:459–468.

Senawi J, Schmieder D, Siemers B, Kingston T, Herrel A. 2015. Beyond size - morphological predictors of bite force in a diverse insectivorous bat assemblage from Malaysia. Funct Ecol 29:1411–1420.

Shi JJ, Rabosky DL. 2015. Speciation dynamics during the global radiation of extant bats. Evolution 69:1528–1545.

Simmons, N. B. 1998. A reappraisal of interfamilial relationships of bats. In: Kunz TH and Racey PA, editors. Bats: phylogeny, morphology, echolocation and conservation biology. Washington: Smithsonian Institution Press.

Storch G. 1968. Funktionsmorphologische Untersuchungen an der Kaumuskulatur und an korrelierten Schadelstrukturen der Chiropteren. Kramer.

Vickerton P, Jarvis J, Jeffery N. 2013. Concentration-dependent specimen shrinkage in iodine-enhanced microCT. J Anat 223: 185–193.